Dedicated to Prof. Dr. S.A. Moskalenko and Prof. Dr. V.A. Moskalenko on the occasion of their 80th anniversary

REVIVAL OF RABI OSCILLATIONS IN OPTICALLY EXCITED SEMICONDUCTOR QUANTUM DOTS

M.D. Croitoru[1], A. Vagov [2], V.M. Axt[2], T. Kuhn[3]

[1]*EMAT, Department of Physics, University of Antwerp, 171, Groenenborgerlaan, B-2020, Antwerp, Belgium*
[2]*Institut für Theoretische Physik III, Universität Bayreuth, Germany*
[3]*Institut für Festkörpertheorie, Westfälische Wilhelms-Universität Münster, Germany*
(Received 24 April 2008)

We present the theoretical investigation of the dynamics of strongly confined laser driven semiconductor quantum dots coupled to phonons. We provide a formally exact solution of this non-Markovian quantum decoherence problem. The method is based on the discrete time-dependent path-integral Monte Carlo technique. This method allows us to explore the cases of long pulses, arbitrary dot-phonon and dot-laser coupling and high temperatures, which up to now have been inaccessible. We find that although Rabi oscillations of the density matrix are suppressed due to phonon induced dephasing, the dephasing rate is a non-monotonic function of the laser field and that it becomes smaller at larger fields leading to a remarkable revival of the Rabi oscillations. This revival is of a general nature which for the type of systems studied here occurs for all temperatures and carrier-phonon coupling strengths.

1. Introduction

Achieving of coherent manipulation of exciton states in semiconductor nanosize quantum dots (QD) is vital for applications in quantum communication and information [1]. The practical implementation requires surmounting several formidable obstacles. The greatest challenge is to preserve the quantum information in the memory for a sufficiently long time to perform all the quantum processing. This stems from the fact that the slightest influence from the environment can cause quantum processors to break down, a phenomenon called decoherence [2]. In "quantum dot under the external laser field systems" the coherence of the carrier states is destroyed and the Rabi oscillations decay even in a single QD [3-5]. Therefore, while quantum dot qubits are rather easily addressable from the outside, they are, in turn, also rather fragile for various decoherence mechanisms from the environment. Interface dots, e.g., typically exhibit a strong radiative decay due to large dipole couplings [3]. Tunneling induces dephasing when Rabi oscillations are measured in the photocurrent [4, 6]. Also off-resonant wetting layer states may contribute to the decay [5, 6]. The coupling of phonons to the QD provides a basic dephasing mechanism, which is present in any sample and all setups and thus marks a lower limit for the total decoherence [7-9]. In typical self-assembled QDs it is indeed the elastic phonon scattering, usually referred to as pure dephasing, which dominates the loss of coherence on a picosecond time scale at temperatures below ~100 K. A theory taking pure dephasing as the only source for decoherence yielded quantitative agreement with experiments in this regime essentially without adjustable parameters [10]. Also the focus of the present work is on the properties of this important mechanism.

For strongly confined dots excited exciton levels can be neglected and a theoretical description can be reduced to a two-level independent boson model (TLIB) coupled to an external field [11]. However, even for this simple quantum dissipative model fully non-perturbative analysis is possible only in the case of ultra-short laser pulses, when the dynamics during the pulse is decoupled from a subsequent free evolution [7]. In the case of arbitrary shaped excitation pulses both perturbation approach [12] and correlation expansion [8] for the TLIB demonstrated the decay of the Rabi oscillations. The obtained results are essential for an important practical problem of reducing the phonon induced decoherence by taking optimal configurations of the driving pulses [13, 14]. The disadvantage of both approaches is that the dot-phonon coupling is assumed small so they are unsuitable to study the cases of strong coupling and large temperatures. In additions, the validity of the methods is questionable for a long time evolution. Dynamics of the system at arbitrary conditions is often studied within the Markovian approximation, which neglects the memory effects introduced by the phonons [5, 6]. However, the analysis of the influence of the induced memory revealed considerable differences with the purely Markovian dynamics [7, 8].

Here we report results for the dynamics of the quantum dots described by the TLIB model that are obtained using the numerical real-time path integral techniques. Path integration is a popular tool in the studies of quantum dissipative systems to which the TLIB model belongs [15]. However, numerical calculations of the path integrals are rather non-trivial for the well known reason that two many paths of nearly equal weigh but random phases can contribute in the calculations. It has recently been shown that this problem can be efficiently solved in the situation when the memory time introduced by the phonon subsystem is finite [16]. In this case the path integral can be reformulated as a pseudo-Markovian evolution of the so-called augmented density matrix. Here we apply a modification of this formalism combined with the "on-fly" path selection algorithm [17-19] to study dynamics and Rabi oscillations of the quantum dots. We obtain numerically accurate dynamics of the system and study previously inaccessible regime of long evolution times and high temperatures.

2. Model and its solution

The TLIB Hamiltonian coupled with the resonant laser field is written in the rotation wave approximation as (expressed in the Bohr units)

$$H = \left(\sigma_z + \frac{1}{2}\right)\Omega + \left(\sigma_z + \frac{1}{2}\right)\sum_q \gamma_q \left(b_q^+ + b_q\right) + \sum_q \omega_q b_q^+ b_q + M\,E(t)\sigma_+ + M^* E(t)\sigma_-, \quad (1)$$

where σ_z, $\sigma_\pm = \sigma_x \pm i\sigma_y$ are Pauli matrices acting on the QD states space, Ω is energy gap between the QD states, b_q (b^+_q) bare annihilation (creation) operators of a phonon with momentum q, ω_q is phonon dispersion, γ_q is the phonon-dot coupling constant, $M_\pm$ is the dot-field coupling constant and $E(t) = f(t)exp[i\Omega t]$ is external laser field of a frequency

$$\overline{\Omega} = \Omega - \sum_q \left(\left|\gamma_q\right| / \omega_q\right)^2,$$

where $f(t)$ is an envelope function, assumed real for simplicity. For our calculations we account only for the coupling with the LA phonons, which provides the most important contribution to the dephasing in the system [7, 20]. The dynamics of the complete density matrix, which includes both dot and phonon states, is obtained by solving the Heisenberg equation

$$i\frac{d\rho}{dt} = \left[H, \rho\right] \quad (2)$$

The initial condition for this equation is obtained from the fact that before the arrival of the pulse the system is in a temperature equilibrium state, for which the density matrix is a direct product of the initial density matrix of the dot states and the phonon temperature distribution

$$\rho(0)=\overline{\rho}(0)\otimes\frac{1}{Z}\prod_{q}\sum_{n_q=0}^{\infty}\exp\left[-\frac{1}{T}n_q\omega_q\right],\quad \overline{\rho}(0)=\begin{pmatrix}0 & 0\\ 0 & 1\end{pmatrix}, \tag{3}$$

where T denotes temperature and Z is the normalization factor. A formal solution of Eq. (2) is written as

$$\rho(t)=U(t)\rho(0)U(t)^{-1} \tag{4}$$

where evolution operator is defined as a time ordered exponent

$$U(t)=\hat{T}\exp\left[-i\int_0^t H(\tau)d\tau\right]. \tag{5}$$

To obtain the reduced density matrix for the dot states we calculate the trace of Eq. (4) over the phonon states. For the TLIB model (1) this trace can be calculated explicitly leading to the well known Feynman-Vernon functional. [21] After that we get the matrix element of the reduced density operator at time t in the space of the relevant system coordinate augmented by a non-local influence functional in the following form

$$\overline{\rho}^{d}_{\sigma_N^+\sigma_N^-}=\sum_{\sigma_0^\pm\ldots\sigma_{N-1}^\pm}R_N\left(\sigma_N^\pm\ldots\sigma_0^\pm\right), \tag{6}$$

where

$$R_N\left(\sigma_N^\pm\ldots\sigma_0^\pm\right)=\prod_{m=1}^{N}M^{+}_{\sigma_m^+\sigma_{m-1}^+}M^{-}_{\sigma_m^-\sigma_{m-1}^-}\exp\left[-\sum_{m}^{N}\left(\sigma_m^+-\sigma_m^-\right)\sum_{j=0}^{m}\left(K_{mj}\sigma_j^+-K_{mj}^{*}\sigma_j^-\right)\right]\overline{\rho}^{(0)}_{\sigma_0^+\sigma_0^-}.$$

with $t = N\Delta$, N is the number of steps, Δ is the time discretization, $t_j = j\Delta$ are discrete time instants, $\sigma_n^\pm = 0,1$, K_{ij} is the memory kernel given in Ref. [22]

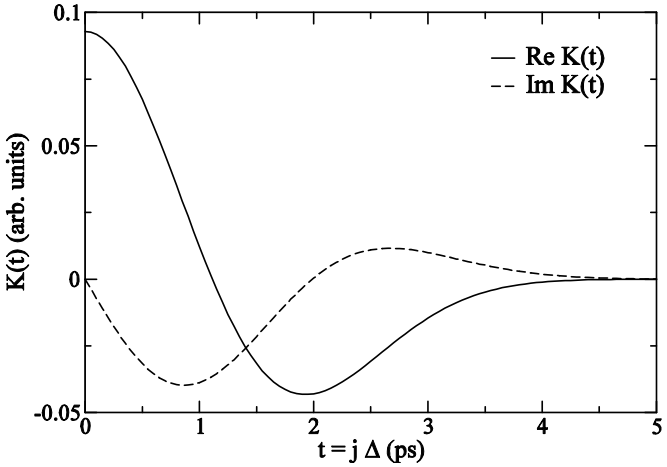

Fig. 1: Time dependence of the memory kernel *K(t)* for a 5 nm spherical GaAs quantum dot at temperature $T = 10$ K.

Equation (6) constitutes a discretized form of the reduced density matrix dynamics of the relevant system and thus provides a starting point for PIMC simulations. To perform path integration of Eq. (6) numerically we employ a modified version of the augmented density matrix algorithm [16], supplemented with the method of "on-fly screening" [17]. The above

described formulation resulted in a path integral over the relevant system paths with an action that is non-local in time. Although the evolution of the reduced density matrix is not Markovian in this case, we note that the memory kernel K_{ij} depends only on the differences i - j. For a quantum dot coupled to a continuum, like the one provided by LA phonons, K_{ij} rapidly decreases with increasing $m = i - j$

$$\lim_{m\to\infty} \mathrm{Re}(K_m) \propto \exp\left[-m^2\varepsilon^2\omega_0^2\right] \tag{7}$$

A graphical illustration of the memory kernel is given in Fig. 1. The additional investigations show that the memory kernel has the finite length independent of the system-bath coupling strength γ_q. We therefore conclude that the system exhibits an effective memory length τ_m such that $K\ (t > \tau_m) = 0\ (I - j > n_{max})$ is a good approximation.

From Eq. (6) we note that there exist the relation between R_N and R_{N-1}

$$R_N\left(\sigma_N^{\pm}\ldots\sigma_0^{\pm}\right) = M^{+}_{\sigma_N^{+}\sigma_{N-1}^{+}} M^{-}_{\sigma_N^{-}\sigma_{N-1}^{-}} \exp\left[-\left(\sigma_N^{+}-\sigma_N^{-}\right)\sum_{j=0}^{N}\left(K_{Nj}\,\sigma_j^{+}-K_{Nj}^{*}\,\sigma_j^{-}\right)\right] R_{N-1}\left(\sigma_{N-1}^{\pm}\ldots\sigma_0^{\pm}\right) \tag{8}$$

This allows us to construct an iterative scheme as follows. At time $t = 0$ we start propagation of the reduced density matrix and get the following result for the density matrix for $t = \varepsilon$.

$$\rho^{d}_{\sigma_1^{+}\sigma_1^{-}} = \sum_{\sigma_0^{\pm}} M^{-}_{\sigma_1^{-}\sigma_0^{-}} M^{+}_{\sigma_1^{+}\sigma_0^{+}}\ I\left(\sigma_1^{\pm},\sigma_1^{\pm}\right) I\left(\sigma_1^{\pm},\sigma_0^{\pm}\right) \rho^{d}_{\sigma_0^{+}\sigma_0^{-}}, \tag{9}$$

where we have introduced the memory interaction function

$$I\left(\sigma_i^{\pm},\sigma_j^{\pm}\right) = \exp\left[-\left(\sigma_i^{+}-\sigma_i^{-}\right)\left(K_{ij}\,\sigma_j^{+}-K_{ij}^{*}\,\sigma_j^{-}\right)\right] \tag{10}$$

For each time step we calculate the complex weights of the all possible paths according to the equation

$$W_i^{1} = M^{-}_{\sigma_1^{-}\sigma_0^{-}} M^{+}_{\sigma_1^{+}\sigma_0^{+}} \prod_{k=0}^{1}\prod_{k'=0}^{k} I\left(\sigma_k^{\pm},\sigma_{k'}^{\pm}\right) \rho^{d}_{\sigma_0^{+}\sigma_0^{-}}, \tag{11}$$

where $i = 1, \ldots, 2^4$ counts the path number.
At the time step m we have

$$\rho^{d}_{\sigma_m^{+}\sigma_m^{-}} = \sum_{i=1}^{L^{(m-1)}} M^{+}_{\sigma_m^{+}\sigma_{m-1}^{+}} M^{-}_{\sigma_m^{-}\sigma_{m-1}^{-}} \prod_{k=0}^{m} I\left(\sigma_m^{\pm},\sigma_k^{\pm}\right) R_{m-1}\left(\sigma_{m-1}^{\pm}\ldots\sigma_0^{\pm}\right). \tag{12}$$

with $L^{(m)} = 2^{2m}$ the number of the all possible path configurations at the time step m, where $m < n_{max}$. Here, we have defined R_N not as a function of variables $\sigma_N^{\pm}\ldots\sigma_0^{\pm}$ but as a function of "paths" on those variables defined as a configuration, e.g. 0,1,0,…1. The corresponding complex weights are

$$W_i^{m} = M^{+}_{\sigma_m^{+}\sigma_{m-1}^{+}} M^{-}_{\sigma_m^{-}\sigma_{m-1}^{-}} \prod_{k=0}^{m}\prod_{k'=0}^{k} I\left(\sigma_k^{\pm},\sigma_{k'}^{\pm}\right) \rho^{d}_{\sigma_0^{+}\sigma_0^{-}}. \tag{13}$$

We see that the number of configurations $L^{(m)}$ grows exponentially. In order the algorithm will be amenable for calculation we employ a Monte Carlo procedure to filter out at each iteration the path configurations with exponentially small contributions at each iteration [17]. This is so called the algorithm of the "on-fly screening". In this procedure, on each iteration step m of Eq. (12) we probe all new values of $\sigma_m^{\pm}$ and select only those values, for which the configuration complex weights larger than a the adopted threshold δ, *i.e.* $W_i^m > \delta$, and store in the memory these values together with the corresponding path configurations. The paths with the complex weights smaller than the given threshold are ignored in the consequent time-point's calculations of the reduced density matrix. This "on-fly" selection procedure provides a considerable decrease of the number of the paths considerably increasing the calculation speed.

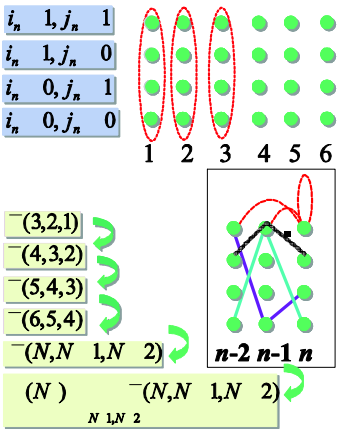

Fig. 2: The schematic representation of the finite memory effect in the density matrix evolution. The circles indicate the levels of the relevant system propagating in the forward and backward directions $n_{lines} = 2^2$. The dashed elliptic lines show the time points excluded from the memory interaction function at time 6ε. The bottom part of the figure shows how the arguments of the reduced density matrix evolve (reindex) with time. The drop of an argument in the density matrix corresponds to a remove of the time-line in the upper part of the figure. For simplicity, only the case of $n_{max} = 2$ is shown. Inset: Schematic representation of the memory interactions (curved lines), which are included in the influence functional at time nε.

The finite bath memory effect reduces the interval of the running variable k in the summation in the exponent of Eq. (8) to the interval $m - n_{\max} \le k \le m$. Then variables $\sigma^{\pm}_{m-n_{\max}} \ldots \sigma^{\pm}_{0}$ are unaffected by the phonon memory and the corresponding functional dependence can be eliminated without information loss by applying the summation over variables $\sigma^{\pm}_{m-1-n_{\max}} \ldots \sigma^{\pm}_{0}$ and introducing the *truncated augmented matrix* as

$$\overline{R}_m\left(\sigma^{\pm}_m \ldots \sigma^{\pm}_{m-n_{\max}}\right) = \sum_{\sigma^{\pm}_0 \ldots \sigma^{\pm}_{m-n_{\max}-1}} R_m\left(\sigma^{\pm}_m \ldots \sigma^{\pm}_0\right), \tag{14}$$

Eq. (8) can be rewritten in a form of a sequence

$$\overline{R}_m\left(\sigma^{\pm}_m \ldots \sigma^{\pm}_{m-n_{\max}}\right) = M^{+}_{\sigma^{+}_m \sigma^{+}_{m-1}} M^{-}_{\sigma^{-}_m \sigma^{-}_{m-1}} \sum_{\sigma^{\pm}_{m-n_{\max}}} \prod_{k=m-n_{\max}}^{m} I\left(\sigma^{\pm}_m, \sigma^{\pm}_k\right) \overline{R}_{m-1}\left(\sigma^{\pm}_{m-1} \ldots \sigma^{\pm}_{m-n_{\max}}\right) \tag{15}$$

If we look at the matrix $\overline{R}_m\left(\sigma^{\pm}_m \ldots \sigma^{\pm}_{m-n_{\max}}\right)$ as at the function of the certain finite path segment $\left(\sigma^{\pm}_m \ldots \sigma^{\pm}_{m-n_{\max}}\right)$ we see that Eq. (15) couples the segment $\left(\sigma^{\pm}_m \ldots \sigma^{\pm}_{m-n_{\max}}\right)$ only to its nearest neighbor $\left(\sigma^{\pm}_{m-1} \ldots \sigma^{\pm}_{m-n_{\max}}\right)$. Therefore, Eq. (15) reminds a Markovian process where the function depends only on this function on the previous step. From the numerical point of view Eq. (15) provides a significant reduction of the memory required to store the augmented density matrix. Fig. 2 illustrates the just described procedure. Another advantage of this representation is that calculation of the evolution requires a single run of sequence (15). The values of the reduced density matrix at $t = t_N$ are obtained as

$$\overline{\rho}(t_N) = \sum_{\sigma^{\pm}_{N-1} \ldots \sigma^{\pm}_{N-n_{\max}}} \overline{R}_N\left(\sigma^{\pm}_N \ldots \sigma^{\pm}_{N-n_{\max}}\right). \tag{16}$$

Finally we note that the memory function K_n satisfies an exact relation

$$\lim_{N\to\infty}\left[\sum_{n=0}^{N} \mathrm{Re}\left(K_n\right) - i\delta\Omega\,\Delta N\right] = 0, \tag{17}$$

which has to be also retained for its finite memory approximation as

$$\sum_{n=0}^{N} \mathrm{Re}\left(K_n\right) - i\delta\Omega\,\Delta N = 0.$$

Apart from discretization errors one can obtain numerically exact results for the full range of model parameters using this algorithm. At higher T, Re(K) is larger and the methods works even better. No numerical difficulties were encountered but very strong fields require smaller time slices and larger computer memory.

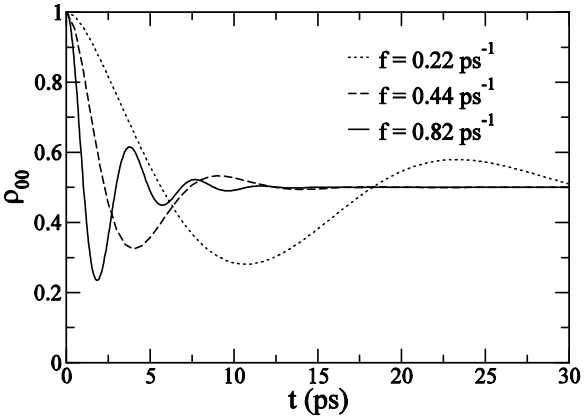

Fig. 3: Time evolution of ρ_{00} of InGaAs dots of d = 10 nm at T = 50 K driven by the external field of selected amplitudes; the case of smaller amplitudes.

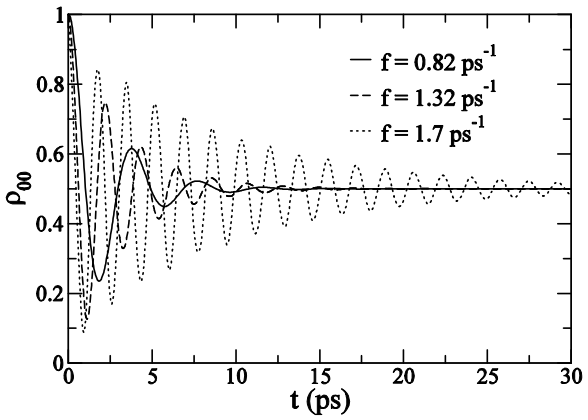

Fig. 4: Time evolution of ρ_{00} of InGaAs dots of d = 10 nm at T = 50 K driven by the external field of selected amplitudes; the case of larger amplitudes.

3. Results and discussion

For the numerical calculations are done for InGaAs quantum dots of a spherical shape. Details of the model and values of the material parameters for the dot-phonon coupling can be found elsewhere Vagov, while the dot diameter is chosen 10nm. The threshold value for rejecting the paths is chosen $\delta = 10^{-8}$. The domain of approximately non-zero K_n is approximately 4ps and $K_{n>4ps/\Delta}$=0. We assume rectangular driving pulses $f(t) = const$, which allows for a transparent physical interpretation while being qualitatively general.

The dynamics of the ρ_{00} density matrix element calculated at T = 50 K for selected values of $f = const$ is illustrated in Fig. 3 for smaller field amplitudes and in Fig. 4 for larger ones. In the Figs. 3 - 4 one sees that Rabi oscillations of the occupation decay to the equilibrium value $\rho_{00} = \rho_{11} = 0.5$. The decay rate noticeably depends on the amplitude of the applied field, moreover this dependence is non-monotonous. For the smaller field amplitudes as shown in Fig. 3 the decay rate increases with the increasing amplitude. However, as seen in Fig. 4 with the further increase in the amplitude the decay rate decreases considerably.

The dynamics of the TLIB in Figs. 3 - 4 is a complicated function of time. In order to extract its effective decay rate quantitatively we approximate it with a simple exponential expression

$$\rho_{00}(t) = \frac{1}{2}\left[1 - \cos(\omega t)\exp(-t/t_d)\right], \tag{18}$$

where ω and t_d are chosen from the best fit of the numerical solution. It turns out that Eq. (18) provides a quantitatively accurate description for the numerically obtained dynamics, while extracted t_d and ω serves as quantitative measures of the decay time and the Rabi frequency of the dot dynamics. Results of the t_d as a function of the applied field obtained at three temperatures T = 10, 50, 100 K are shown in Fig. 5.

At all selected temperatures t_d is a non-monotonous function of the field. For the smaller fields the decay time decreases with the increasing field before reaching its minimum at $f \approx 1ps^{-1}$. We note that the inverse of this value is approximately equal to the kinetic time in the phonon subsystem, which for the chosen parameters is $\tau \approx$ 1ps.

As seen in Fig. 5 the decay time increases at the increased temperatures. Fig. 6 shows the decay time as a function of the temperature for two values of the field, chosen from different domains of the $t_d(f)$ function. In both cases the decay time decreases at increased temperatures, which appear intuitively justified.

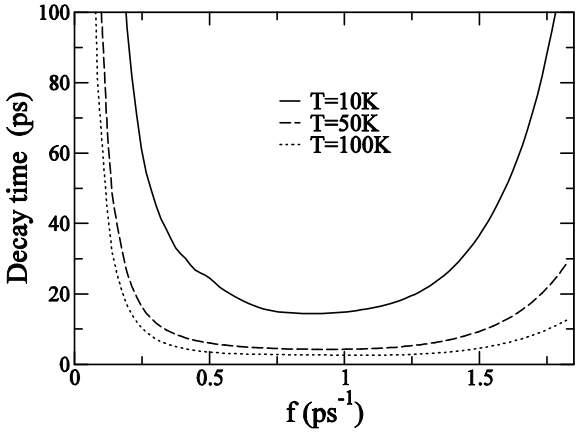

Fig. 5: Decay time t_d as a function of the field amplitude obtained by fitting numerical results with Eq. (18).

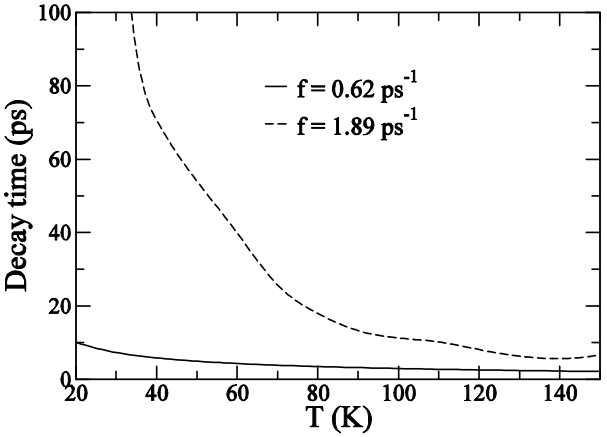

Fig. 6: Decay time t_d as a function of the temperature obtained by fitting numerical results with Eq. (18).

Effective frequency ω (or the period) of the Rabi oscillations is another important characteristics of the system. As is well known, in the absence of the phonon coupling ω is proportional to the field f and is temperature independent. When the phonon coupling is present the situation is strikingly different as demonstrated in Figs. 7 and 8, which show the normalized period of the oscillations (the period multiplied by f).

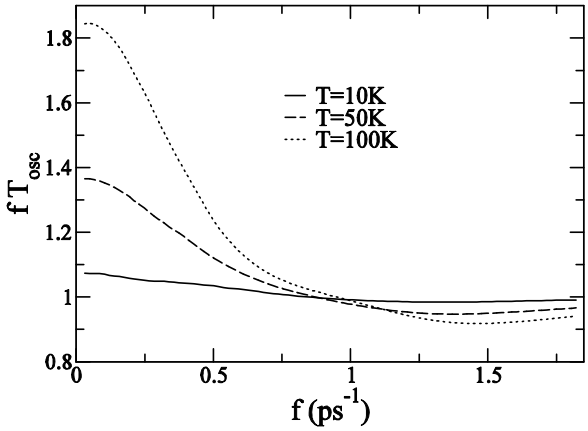

Fig. 7: Normalized period of Rabi oscillations (divided by that period without the phonon coupling) as a function of field obtained by fitting numerical results with Eq. (18).

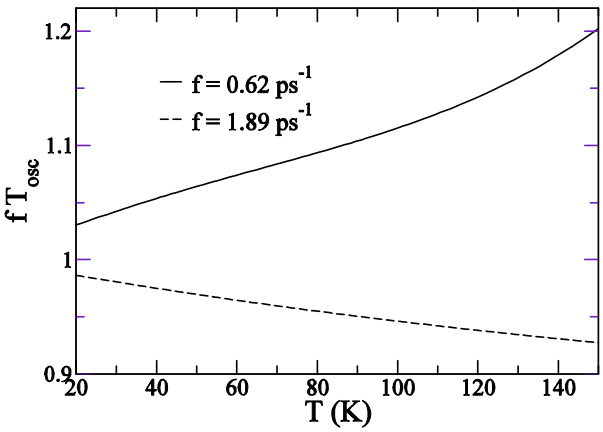

Fig. 8: Normalized period of Rabi oscillations as a function of temperature obtained by fitting numerical results with Eq. (18).

As is seen in Fig. 7 similarly to the decay time, the field dependence of the period can be separated into two different domains $f < 1\text{ps}^{-1}$ and $f > 1\text{ps}^{-1}$, with a considerably different behavior. In the first domain, $f < 1\text{ps}^{-1}$, the normalized period exceeds unity, which means that the period is increased by the phonon coupling. This increase is considerably larger at higher temperatures. In the other domain, $f > 1\text{ps}^{-1}$, the influence of the phonon coupling produces the opposite effect: the period is decreased. The decrease is of a less magnitude than that in the first domain, but it is also more pronounced at the higher temperatures. Fig. 8 illustrates the temperature dependence of the normalized period. For two field values from the two domains the effect of the temperature influence is opposite: for the domain of the smaller fields the period increases, while for that of the larger fields the period decreases.

The increase of the period at the smaller fields can be understood by calculating Eq. (6) in the limit $f \to 0$ which yields the infinite decay time and an exact analytical expression for the normalized period of the Rabi oscillations

$$T = 2\pi \exp\left[\sum_q \frac{|\gamma_q|^2}{\omega_q^2}\left(1+2N_q\right)\right] \underset{T\tau_{ph}>>1}{\to} 2\pi \exp\left[2T\sum_q \frac{|\gamma_q|^2}{\omega_q^3}\right]. \tag{19}$$

Hence in the limit of vanishing fields the period exponentially increases at the increased phonon coupling constant and temperatures. This is expected to hold for small finite field amplitudes. The decay time in the domain of small fields in Fig. 3 is indeed quite large in agreement with this result.

The fact that the critical field separating two domains is approximately equal to the energy scale, defined as the inverse of the phonon kinetic time τ_{ph} is not accidental. Rabi rotations effectively introduce an energy scale equal to its frequency ω into the system. This has to be compared with the characteristic energy of the phonon subsystem, which is estimated as τ_{ph}^{-1}. One could also expect that the phonon coupling influence on the dynamics reaches its maximum when the two energies coincide and that the influence diminishes when $\omega >> \tau_{ph}^{-1}$. This coincides with what is obtained in the calculations. This intuitive reasoning can be supplemented with the results obtained by the perturbative calculations [12], according to which the evolution of $\rho_{11} = 1\text{-}\rho_{00}$ is given by [23]

$$\rho_{11}(t) = -\int_{-\infty}^{\infty} \frac{R(\omega)}{\omega^2} S(\omega,t) \tag{20}$$

where $R(\omega)$ is the spectral density of the phonon reservoir coupled to the QD while $S(\omega,t)$ defines optically controlled dynamics and can be represented as a sum of $\delta S(\omega,t)$ and ω independent expression $\sin(2f\tau)^2/4$. According to Eq. (20) the decay rate of the oscillations depends on the overlap between $\delta S(\omega)$ and $\delta R(\omega)/\omega^2$. It can be demonstrated that for the chosen dot model $R(\omega)$ has its maximum near $\omega = 0$ and decays exponentially with the rate $\propto \tau_{ph}^{-1}$. At the same time for a rectangular shaped pulse $\delta S(\omega)$ is found as

$$\delta S(\omega) = \frac{f^2}{4}\left|\frac{\exp[i(\omega+f)t]-1}{\omega+f} + \frac{\exp[i(\omega-f)t]-1}{\omega-f}\right|^2. \tag{21}$$

It can be demonstrated [12] that this function has a multi-peak structure. The largest of those peaks is found at $\omega = f$ and shifts to the right when f increases. At $f >> \tau_{ph}$ the overlap becomes negligible leading to the diminishing phonon influence on the dynamics which explains the origin of the Rabi oscillations revival.

Conclusions

We have presented results of the numerical calculations of the dynamics of quantum dots resonantly excited by rectangular laser pulses, which demonstrated several interesting and unexpected phenomena. It was shown that although the Markovian approximation with constant damping can satisfactory approximate the dynamics at chosen field and temperature, its fails to predict the change of the damping constant with the field amplitude and the system temperature. Moreover, we have indicated that the phonon coupling leads to a considerable renormalization of the period of Rabi oscillations.

Obtained field dependence of the decay time and the period is shown to separate into two distinctive domains of the smaller and larger field amplitude, in which their behavior differs considerably. While for the smaller fields the decay rate increases at the increased field, at the larger fields the opposite trend is observed leading to the revival of Rabi oscillations. The domains also differ by the field and temperature dependence of the oscillations period. While in the smaller fields domain the period exceeds that in the absence of the phonon coupling and increases at the higher temperatures, in the larger fields domain it is smaller than that in the absence of the phonon coupling and further decreases at the high temperatures.

Finally we note that an appearance of the two domains in the field dependence of the dynamics seems to be a general phenomenon, not related to a particular choice of the dot model and of the dot-phonon coupling. This can be explained by the overlap of the effective energy scales in the system, introduced by the Rabi oscillations and by the phonon coupling. Consequently, the revival of the Rabi rotations at large fields can occur in many physical realizations of the dissipative quantum mechanical systems.

References

[1] E. Biolatti, R.C. Iotti, P. Zanardi, and F. Rossi, Phys. Rev. Lett., 85, 5647, (2000); F. Troiani, U. Hohenester, and E. Molinari, Phys. Rev. B, 62, R2263, (2000).
[2] D. DiVincenzo and B. Terhal, Decoherence: the obstacle to quantum computation, Physics World, March, 53, (1998).
[3] T.H. Stievater et al., Phys. Rev. Lett., 87, 133603, (2001).
[4] S. Stufler, P. Ester, and A. Zrenner, Phys. Rev. B, 72, 121301(R), (2005).
[5] Q.Q. Wang et al., Phys. Rev. B, 72, 035306, (2005).
[6] J.M. Villas-Bôas, Sergio E. Ulloa, and A.O. Govorov, Phys. Rev. Lett., 94, 057404, (2005).
[7] A. Vagov, V.M. Axt, and T. Kuhn, Phys. Rev. B, 66, 165312, (2002).
[8] J. Förstner, C. Weber, J. Danckwerts, and A. Knorr, Phys. Rev. Lett., 91, 127401, (2003).
[9] E.A. Muljarov, T. Takagahara, and R. Zimmermann, Phys. Rev. Lett, 95, 177405, (2005).
[10] A. Vagov et al., Phys. Rev. B, 70, 201305, (2004).
[11] A. Vagov, V.M. Axt, T. Kuhn, W. Langbein, P. Borri, and U. Woggon, Phys. Rev. B, 70, 201305, (2004).
[12] P. Machnikowski and L. Jacak, Phys. Rev. B, 69, 193302, (2004).
[13] V.M. Axt, P. Machnikowski, and T. Kuhn, Phys. Rev. B, 71, 155305, (2005).
[14] U. Hohenester and G. Stadler, Phys. Rev. Lett., 92, 196801, (2004).
[15] A.J. Leggett et al., Rev. Mod. Phys., 59, 1, (1987).
[16] N. Makri and D. Makarov, J. Chem. Phys., 102, 4600, (1995); ibid. 102, 4611, (1995).
[17] E. Sim, J. Chem. Phys., 115, 4450, (2001).
[18] E. Sim and N. Makri, Chem. Phys. Lett., 249, 224, (1996).
[19] E. Sim and N. Makri, Comput. Phys. Commun., 99, 335, (1997).
[20] B. Krummheuer, V.M. Axt, and T. Kuhn, Phys. Rev. B, 65, 195313, (2002).
[21] R.P. Feynman and F.L. Vernon, Annals of Physics, 24, 118, (1963).
[22] A. Vagov, M.D. Croitoru, V.M. Axt, T. Kuhn, F.M. Peeters, Phys. Rev. Lett., 99, 227403, (2007).
[23] A. Krügel et al., Appl. Phys. B, 81, 897, (2005).